1 *Article*

2 # Accuracy Assessment on Unmanned Aerial System
3 # Derived Digital Surface Models

4 **Salvatore Manfreda [1], Petr Dvorak [2], Jana Mullerova [3], Sorin Herban [4], Pietro Vuono [5], José Juan**
5 **Arranz Justel [6], Matthew Perks [7]**

6 [1] Dipartimento delle Culture Europee e del Mediterraneo: Architettura, Ambiente, Patrimoni Culturali
7   (DiCEM), Università degli Studi della Basilicata, 75100 Matera, Italy; salvatore.manfreda@unibas.it
8 [2] Institute of Aerospace Engineering, Brno University of Technology, Technicka 2, 61669 Brno, Czech
9   Republic; dvorak.p@fme.vutbr.cz
10 [3] Department GIS and Remote Sensing, Institute of Botany of the Czech Academy of Sciences, 252 43
11   Pruhonice, Czech Republic.; jana.mullerova@ibot.cas.cz
12 [4] Poliltehnic University of Timisoara, Traian Lalescu 2°, 300223 Timisoara, Romania; sorin.herban@upt.ro
13 [5] Scuola di Ingegneria, Università degli Studi della Basilicata, 85100 Potenza, Italy; pietro.vuono@unibas.it
14 [6] ETSI Topografía, Geodesia y Cartografía, Universidad Politécnica de Madrid; josejuan.arranz@upm.es
15 [7] School of Geography, Politics and Sociology, Newcastle University, Newcastle upon Tyne NE1 7RU, UK;
16   matthew.perks@newcastle.ac.uk

17
18 * Correspondence: salvatore.manfreda@unibas.it; Tel.: +39-0971 205139

19

20 **Abstract:** Small unmanned aerial systems (UAS) represent a cost-effective strategy for topographic
21 surveys. These low-cost drones can provide useful information for 3D reconstruction even if they
22 are equipped with a low-quality navigation system. To ensure the production of high-quality
23 topographic models, careful consideration of flight mode and proper distribution of ground control
24 points is required. To this end a commercial drone has been adopted to monitor a small earthen
25 dam using different combinations of flight configurations and adopting a variable number of
26 ground control points (GCPs). Results highlighted that both choice and combination of flight plans
27 can reduce the relative error of the 3D model up to a few meters without the need of including
28 GCPs. The use of GCPs allows the quality of topographic survey to be greatly improved, reducing
29 error to the order of a few centimeters. In particular, the combined use of images extracted from two
30 flights, one with a camera mounted at nadir and the second with a 20° angle, proves extremely
31 beneficial to increase the overall accuracy of the 3D model and especially of the vertical precision.

32 **Keywords:** Topographic surveys, UAS, DSM, GCPs, SfM, MVS.

33 **1. Introduction**

34   Unmanned aerial systems (UAS) are getting increasingly popular for many environmental
35 applications, delivering frequent and very high-resolution digital surface/elevation models
36 (DSM/DEMs) and orthoimagery [1-3]. High precision is crucial for many applications, especially for
37 change detection studies [e.g. 4, 5]. Traditionally, DSMs are delivered using terrestrial or aerial
38 surveys (laser scanning), which are often time-consuming, difficult to organize, and costly [6].
39 Structure from Motion (SfM) and multi-view stereo (MVS) algorithms allow creation of DSMs and
40 orthomosaics without prior information on camera parameters such as focal length or radial
41 distortion, and provide a flexible and low-cost alternative, enabling high temporal frequency and
42 optimal timing of the mission [7, 8].
43   The accuracy of SfM-derived DSMs is highly variable, and the causes are still not fully
44 understood (see the review by Smith and Vericat [9]). A number of factors may affect precision of
45 UAS-derived orthoimagery and digital elevation data, such as flight parameters (e.g. elevation above
46 ground level - AGL, flight speed, direction, orientation of the camera, camera's focal length, etc.),
47 image quality, processing software, morphology of the studied area, and type of vehicle (fixed or

48 rotary wing). For instance, flight at low altitudes often requires short focal length lenses to be fitted
49 to the camera in order to maintain sufficient coverage of the terrain. These lenses often introduce
50 considerable geometric distortion into the imagery and thus overall accuracy is compromised.
51   It should be also stated that most available SfM software operates like a black-box with several
52 default parameter settings. It has been shown that appropriate settings can reduce positioning error
53 of SfM-MVS products [10], but processing workflow and accuracy assessment methodology need to
54 be optimized and standardized [8, 11].
55   In this context, ground control points (GCPs) are a commonly used to increase the precision of
56 products, even though their collection represents a laborious and time intensive part of UAS
57 campaigns. The literature offers a wide spectra of choices for the number and spatial distribution of
58 GCPs used to support SfM-MVS algorithms. A selection of the most recent publications dealing with
59 the impact of GCPs configurations/number on DSM quality is reported in Table1. Such experiences
60 taken individually do not provide a clear guidance for the identification of the appropriate number
61 of GCPs, but they provide a valuable source of information for the definition of some preliminary
62 guidelines.
63   In particular, we harmonized the information contained in the mentioned refences extracting all
64 available data in terms of DSM planar and vertical accuracy. These data are summarized in Figure 1
65 that describes the measured planar and vertical Root Mean Square Error (RMSE) as a function of the
66 GCPs density. This allows to compare outcomes of different studies and better identify general
67 tendencies. According the analyzed literature, DSM accuracy tends to increase with the number of
68 GCPs adopted reaching rapidly an asymptotic behavior. Commonly for all the experiments, errors
69 observed on the vertical precision are systematically higher compared to the horizontal one. It can be
70 noticed that planar errors decrease more rapidly with the increase of GCPs in comparison to vertical
71 errors. In this graph, the planar error tends to stabilize when the GSP density exceeds 5, while 10
72 GCPs/ha are needed to reach the same condition on vertical precision. This emphasizes the need to
73 find new strategies to improve DSM accuracy especially in elevation estimates.
74

Reference	Area [ha]	Number of GCPs	AGL [m]	$RMSE_{X,Y}$ [cm]	$RMSE_Z$ [cm]	RMSE Total [cm]
Rock et al. [12]	N/A	1042	50-550	N/A	5.5	N/A
Tahar [13]	150	8-9	N/A	50.0	78.0	N/A
Mancini et al. [14]	2.75	18	40	0.8	10.0	N/A
Hugenholtz et al. [15]	4.5	28	200	18	29	N/A
Lucieer et al. [4]	0.75	39	N/A	7.4	6.2	N/A
Cryderman et al. [16]	7.12	11	118	3.3	3.1	4.6
Gómez-Candón et al. [17]	1.0	11-45	30-100	N/A	N/A	0.29-0.12
Uysal et al. [18]	5.0	27	60	N/A	6.62	N/A
Kung et al. [19]	210.0	19	262	38	107	125
Agüera-Vega et al. [20]	17.64	4-15-20	120	7-4.5-1.7	33-5.8-4.7	N/A
Koci et al. [21]	41-45-72	6-7	100	N/A	30.9-68.7-95.9	N/A
James et al. [17]	7.5	4-27	100	4.9-	N/A	1.6
Oniga et al. [22]	1.0	3-40	28-35	4.5-8.9	6.6-4.0	7.4-7.9

75 **Table 1.** Precision of DSMs created using a variable number of GCPs, examples extracted from the
76 literature.

77   The literature review offered useful indications about the optimization of the number of GCPs,
78 but synergic effects of their number and spatial arrangement, as well as flight characteristics are still
79 not fully understood [see 5, 17, 20]. Optimizing UAS campaigns would therefore make an important
80 step towards the effectiveness and reliability of UAS-derived products.
81   In the present manuscript, we explore the impact of both UAS flight characteristics (e.g., altitude,
82 camera tilt, and flight plan) and GCPs density on the accuracy of a 3D model of a small earthen dam.
83 Analyses help understanding the procedure to increase the reliability of digital surface models
84 (DSMs) that represent a critical information in environmental and hydrological science.
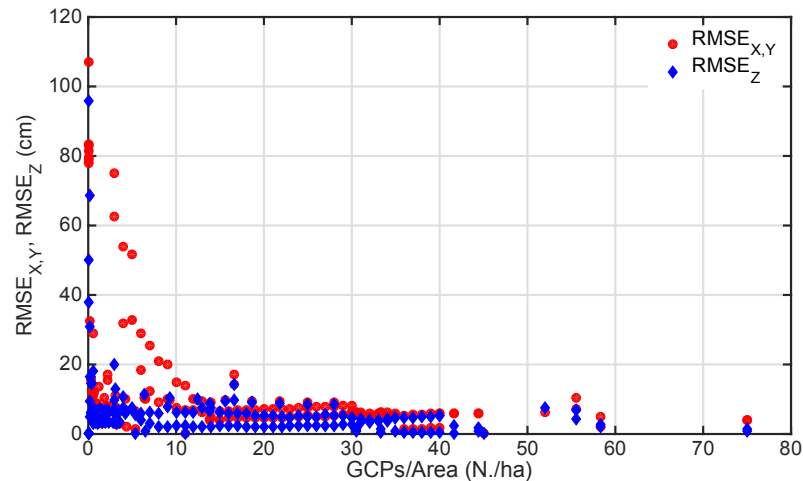
Figure 1. DSM accuracy in terms of planar and vertical RMSE as a function of the GCPs density (data extracted from the literature reported in Table 1).

2. Materials and Methods

2.1. Study area

The survey experiment was executed on an earthen dam next to the village Pișchia, 20 kilometers northwest from Timisoara (western Romania). The Pișchia dam, managed by National Water Administration, has a volume of approximately 500,000 m³, which is used to supply drinking water and for recreation activities (e.g., fishing). It has a trapezoidal cross section with side slope of 1:3 and a maximum elevation of about 10 m. The surrounding area is characterized by agricultural land with gentle slopes (Figure 2).
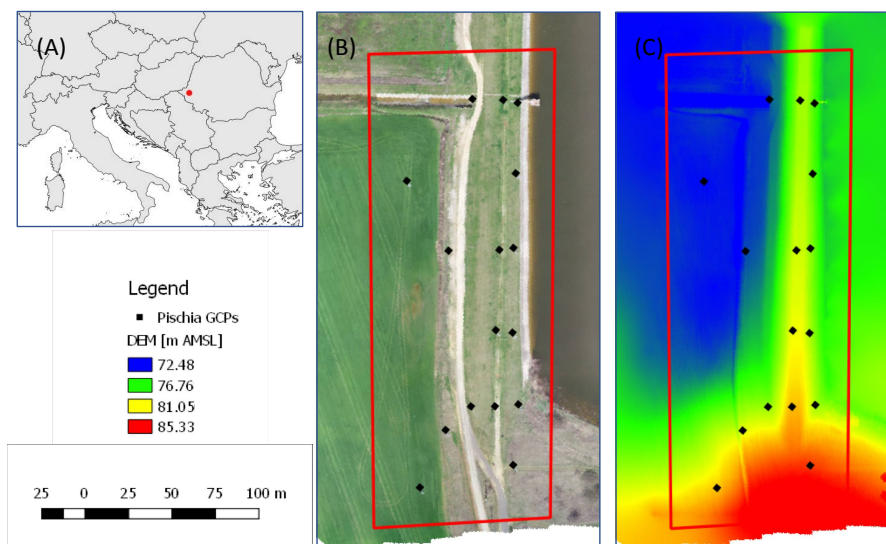
Figure 2. A) Position of the study area within Europe (45.927N, 21.335E). B) Description of the study area and distribution of the GCPs. C) UAS-derived DSM of the area.

2.2. Primary data collection

All flights were performed with DJI Phantom 4 Pro quadcopter, featuring a gimbaled 20 Mpix 1" sensor with mechanical shutter. Focal length of the lens was 24 mm (full-frame equivalent). The data were stored in 24 bit JPG format, pixel size was 2.41 um. Camera sensitivity was set at ISO100 for all images with aperture ranging from 4 to 5.6 and shutter times ranging between 1/120-1/500. All images were georeferenced with the on-board GPS. The WGS84 coordinates were stored in JPG EXIF.

105 Mission planning was executed in Pix4Dcapture that enabled control of the camera tilt. All six flights
106 were performed between 10:00 and 12:50 UTC. Flight missions were planned using side overlap of
107 60%, and a front overlap of 80%.

Fligth	Fligth Plan	Level Above the Ground (m)	Camera Tilt (degree)	Avg GSD (cm/px)	Number of Images
N.1		60	0°	1.9	276
N.2		60	0°	1.9	268
N.3		60	70°	-	271
N.4		60	20°	2.0	273
N.5		60	0°	1.9	257
N.6		120	0°	3.3	85

108

109 **Table 2.** Characteristics of the different surveys carried out during the experiment.

110 In order to explore the impact of mission planning on the overall accuracy of UAS-derived DSM,
111 different flight plans have been performed changing flight trajectories, camera tilt, and elevation of
112 the flight. The variable characteristics of the six flights are summarized in Table 2, while other
113 parameters such as camera settings and additional mission flight settings (e.g., overlap) are kept
114 constant. Some examples of the images obtained by different configurations are shown in Figure 3,
115 where an area from the central part of the dam is reproduced. From these images one can recognize
116 the outlet tower and the spillway of the dam.
117 The survey was carried out on 4th April 2018 between 10:00 and 12:50 UTC. Flights were planned
118 to cover an area of approximately 100 x 270 m (about 2.7 ha), an extent highlighted in Figure 2.B (see
119 red line boundaries). In the same figure, we also report the UAS-derived Digital Surface Model (DSM)
120 of the area.
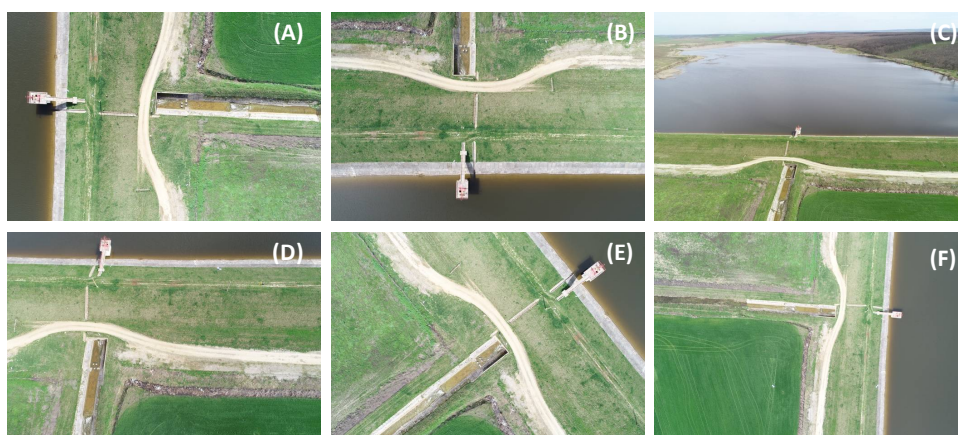
121

122 **Figure 3.** Images of the central part of the dam body acquired during flight N.1 (A), N.2 (B), N.3 (C),
123 N.4 (D), N.5 (E), and N.6 (F).

124 For the aim of the present study, only a portion of the dam has been studied using about 16
125 GCPs distributed along the dam main structure and in the adjacent agricultural area. They have been
126 placed along five longitudinal alignments trying to measure the full range of elevation changes.
127 Maximum vertical variation of GCPs is about 10.6 m.

128 The GCP positions were determined using a Leica 1200 system of RTK GNSS rover and a precise
129 Leica 1201 Total Station with a view to achieve a precision better than 3 mm for all GCPs. To
130 determine a geodetic base, corrections were acquired from the Romanian Position Determination
131 System (ROMPOS) network of GNSS permanent stations.

132 *2.3. Data Processing*

133 Images retrieved by each flight were processed using Agisoft PhotoScan ver. 1.4.3 to derive a 3D
134 model of the area. The same workflow was repeated each time keeping constant the software settings,
135 following sequence of commands: 1) Photo alignment with high accuracy; 2) Optimizing alignment;
136 3) Dense cloud building with high quality + aggressive depth filtering; 4) Mesh building using a
137 sparse cloud; 5) Texture building with default blending mode; 6) Tiled model building; 7) DSM
138 building using default settings; 8) Orthomosaic generation.
139 In a preliminary phase, we focused on the use of the geotagged images alone excluding the use
140 of GCPs. Measured GCPs have been adopted as check points only to validate the results. Elaboration
141 carried out without GCPs allowed us to better understand the role of flight mode and combination
142 of different flights on the resulting DSM. This was made possible by exploring accuracies of DSMs
143 obtained using imagery extracted from a single flight and from the combinations of two flights.
144 Resulting combinations displayed a wide variability in the precision of planar coordinates and
145 elevation. This preliminary analysis allowed identifying the best performing flight configuration and
146 also the benefit due to the use of combined flights.
147 To increase the quality in the 3D model, GCPs can be included in the elaboration for
148 georectification. Number and distribution of GCPs per unit area are not univocally identified in
149 literature as highlighted in the introduction [see e.g., 23]. In fact, the number of GCPs necessary for
150 the survey is influenced by the extent of the study area and its morphology, camera deployed, drone
151 GPS precision, and the type of the survey.
152 According to the analysis carried out without GCPs, two groups of images extracted from a
153 single flight and from two flight missions were selected to explore the role played by the GCPs
154 density and distribution. A random number of GCPs ranging from 1 up to 9 was used in this second
155 phase, while the remaining GCPs were employed as check points. This second analysis was extremely
156 useful to understand the mutual benefit of combination of flights and a well-designed GCP
157 distribution. Proper use of these two settings emphasize the potential of SfM-MVS algorithms in
158 providing good quality DSMs. The comparison between single and multiple flights combined with
159 the use of GCPs was stimulated by the need to better understand the benefits of combining multiple
160 flights.

161 **3. Accuracy assessment of the 3D models**

162 *3.1. Impact of mission planning on DSM*

163 Results of the quality assessment based on individual flights with different settings (for details
164 see Table 2) and their combinations are summarized in Table 3, where we reported the Root Mean
165 Square Error (RMSE) estimated between the 3D model derived by the SfM-MVS algorithms of
166 PhotoScan and the 16 check points distributed in the area. The table provides four groups of
167 information in the following order, starting from the upper part: the planar error of the topographic
168 surface, the absolute elevation, the relative elevation defined as elevation reduced by the minimum
169 value observed among the considered validation points, and the total error obtained as the sum of
170 planar and vertical error. Columns and rows identify the combination of flights adopted for the
171 analysis including single flight configurations reported on the diagonal of each table.
172 These preliminary results summarize the impact of flight configuration on DSM accuracy. It can
173 be observed that the relative error in planar coordinate is significantly lower in respect to the vertical
174 absolute error. In fact, the SfM-MVS estimated elevation is affected by an error of one or two orders
175 of magnitude larger than planar georeferencing. Such a systematic error becomes less critical when
176 taking into consideration the relative elevation of the surface. Another result is represented by the

177 low quality of the 3D models derived with images taken with a camera tilted of 70°. Such a camera
178 configuration produces images with limited amount of information that deteriorates the result in all
179 combinations, especially for planar coordinates. This survey becomes beneficial only in reducing the
180 error of the absolute elevation of the DSM, but its value is limited in terms of relative elevation (see
181 third panel of Table 3).

Planar Coordinates - RMSE$_{X,Y}$ (m)					
Flight	N. 1	N.2	N. 3	N. 4	N. 5	N. 6
N. 1	4.47					
N.2	2.39	2.03				
N. 3	136.05	1497.25	X			
N. 4	**1.64**	3.08	3835.20	7.75		
N. 5	2.09	1.95	15042.56	8.05	7.15	
N. 6	3.06	3.35	1750.11	8.63	6.94	19.70

Elevation - RMSE$_Z$ (m)					
Flight	N. 1	N. 2	N. 3	N. 4	N. 5	N. 6
N. 1	82.90					
N.2	81.18	78.72				
N. 3	80.32	56.94	X			
N. 4	79.21	76.94	15.51	75.02		
N. 5	77.90	77.86	**7.70**	73.35	71.86	
N. 6	78.79	75.48	20.25	72.85	70.27	59.75

Relative Elevation - RMSE$_Z$ (m)					
Flight	N. 1	N. 2	N. 3	N. 4	N. 5	N. 6
N. 1	1.06					
N. 2	0.39	0.37				
N. 3	3.74	19.55	X			
N. 4	0.55	0.42	5.88	**0.11**		
N. 5	0.39	0.25	8.00	0.47	0.26	
N. 6	0.22	0.94	13.85	0.80	0.40	3.44

Planar and vertical - RMSE (m)					
Flight	N. 1	N. 2	N. 3	N. 4	N. 5	N. 6
N. 1	4.59					
N.2	2.42	2.06				
N. 3	136.10	1497.38	X			
N. 4	**1.73**	3.11	3835.20	7.75		
N. 5	2.13	1.97	15042.56	8.06	7.15	
N. 6	3.07	3.48	1750.16	8.67	6.95	20.00

Performances

| High |
| Medium |
| Low |

182 **Table 3.** RMSE estimated on 16 GCPs for planar coordinates, absolute elevation, relative elevation
183 defined as elevation reduced by the minimum value observed among the considered validation
184 points, and the sum of the planar and vertical error obtained using different images taken from
185 different flight combinations (for description see Table 2). The values written in bold represent the
186 best performing configuration for each specific sub-group.

187 The best results in terms of planar coordinates were obtained combining the flights N. 1 and N.
188 4, while the best performances in terms of relative elevation was obtained with the flight N. 4. It can
189 be observed that all combinations including flight N. 4 provided an improvement in the accuracy of
190 the relative elevation. Considering the sum of the planar and vertical errors (considering the relative
191 elevation), the best performing set of images was obtained by the combination of flight N. 1 and N.
192 4. Among the tests based on a single flight, the results obtained with the flight N. 2 provide good
193 results with a total error slightly higher than the best combination of two flights.

3.2. The Use of GCPs in the SfM-MVS processing

195 The required number of GCPs has been investigated using several combinations of GCPs
196 selected from the 16 check points available. Therefore, we tested the planar and vertical accuracy of
197 the 3D model generated using the survey N. 2 and the ensemble of images obtained from the

198 combination of flight N. 1 and 4. Approximately 64 combinations of GCPs, with a variable number
199 ranging from 1 up to 9 (55% of the available check points), have been tested for each dataset providing
200 useful guidelines on the appropriate strategy to improve the overall accuracy of resulting DSMs.

201 *3.2.1. DSM derived from a single flight*

202   In the present section, the accuracy assessment of the DSMs derived using the images from flight
203 N.2 is described. This flight was selected among the many presented in the previous section, because
204 it provided the best accuracy among the single flight options explored (see diagonal values of RMSE
205 in Table 3).
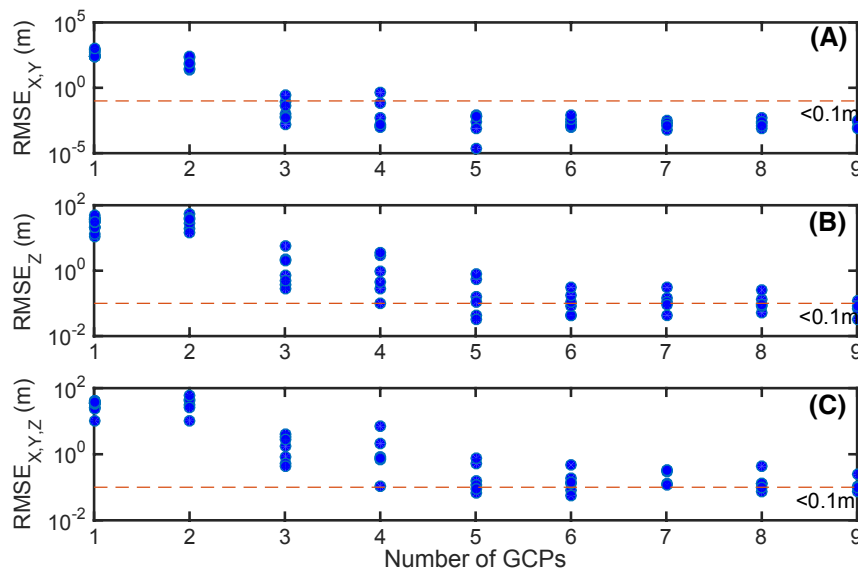
206

207 **Figure 4.** RMSE of the 3D model as a function of the number of GCPs adopted. A) RMSE in planar
208 coordinates; B) RMSE in relative elevation; C) RMSE in X, Y, and Z obtained for the flight N.2.

209   Several DSMs have been generated using different combinations of GCPs modifying their
210 number and relative distribution in space. Results of these analyses are summarized in Figure 4,
211 where a sharp increase in DSM accuracy can be observed moving from 1 – 2 GCPs to 3 – 4 GPCs, with
212 a mean error dropping from tens of meters to few meters only. This result is a well-known outcome
213 due to the need of a minimum of three GCPs for the 3D transformation of coordinates.
214   The magnitude of planar errors is significantly reduced moving from four to five GCPs and
215 seems to be fairly stable after five GCPs. On the other hand, vertical errors are always larger and tend
216 to be more stable after six GCPs. In particular, planar error reaches values of few centimeters adopting
217 only five GCPs (Figure 4), while vertical accuracy ranges from 6 – 74 cm for the same number of
218 GCPs. Therefore the total error of DSM is influenced the most by higher values of $RMSE_Z$.

219 *3.2.2. DSM derived from the combination of two flights*

220   Adopting the combination of two flights the general patterns are similar to those observed in the
221 previous section. Therefore, similar considerations can be made regarding the impact of GCPs
222 numerosity. However, some key differences can be identified. Most notably, the RMSE's are generally
223 lower when two flights of differing configurations are used, especially when more than six GCPs are
224 adopted. In particular, the $RMSE_{X,Y}$ is significantly below the threshold of 10 cm (the dashed line
225 plotted in the graph), when more than 4 GCPs are adopted. $RMSE_Z$ is less than 10 cm when more
226 than six GCPs are adopted. Comparing the results of Figure 4 and 5, it can be noted that the errors in
227 terms of planar coordinates ($RMSE_{X,Y}$) are comparable, but there is a critical difference in the elevation
228 accuracy ($RMSE_Z$). This highlights the relative advantage of introducing two-flight combination in

229   the process, because the nadir orientation provides the best configuration for the planar coordinates,
230   while the 20° tilted camera increases the vertical accuracy (see Table 3 for comparison).

231
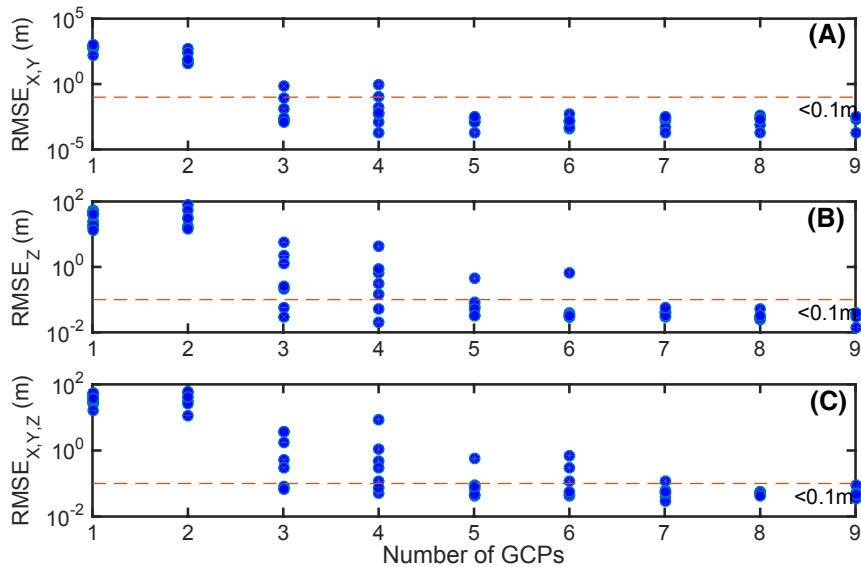
Figure 5. RMSE of the 3D model as a function of the number of GCPs adopted in the model run. A)
RMSE in planar coordinates; B) RMSE in relative elevation; C) RMSE in X, Y, and Z for the
combination of flights N.1 and N.4.

235   In order to emphasize the relative differences between the two configuration explored herein.
236   Results obtained with a single flight and two flights are compared in Figure 6 that highlights the
237   benefits of flight combination in terms of planar (panel A) and vertical (panel B) accuracy. The two
238   configurations display minimal differences in terms of planar accuracy, while the results are
239   significantly improved in the vertical precision when two flights are adopted. The DSMs obtained
240   using a best combination of two flights reaches a vertical accuracy of about 3.5 cm if six or more GCPs
241   are used. Moreover, the results seem to be relatively stable with more than six GCPs.

242
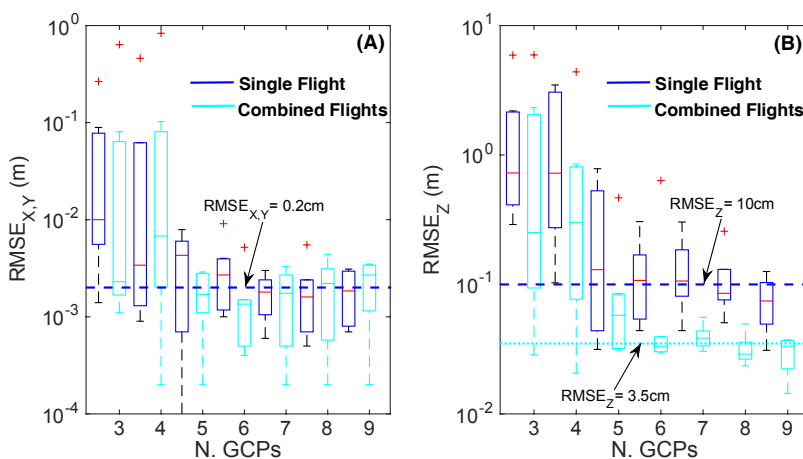
**Figure 6.** Comparison of results obtained changing the number of GCPs and adopting a single flight
or a two flights dataset on the plane (A) and z-axes (B).

245   *3.2.3. The spatial distribution of GCPs*

246   The spatial distribution of GCPs controls strongly the DSM accuracy. Its influence has been
247   explored looking at the relationship between the planar and vertical RMSE and the mean relative

248   distance between the GCPs on the plane (see Figure 7.A, C) and elevation (Figure 7.B, D). The analysis
249   has been carried out for the two cases under investigation: 1) the single fight (Figure 7.A and B) and
250   the combination of two flights (Figure 7.C and D). The RMSE associated with different number of
251   GCPs are plotted using different colors to discriminate between the outputs obtained with different
252   number of GCPs. It can be observed that each group is located in a portion of the graph (upper or
253   lower) according to the number of GCPs. More GCPs the lower is generally their position on the
254   graph. Nevertheless, all groups show a clear decrease of the errors with the increase of the mean
255   distance both on the plane and on the z-axis.

256
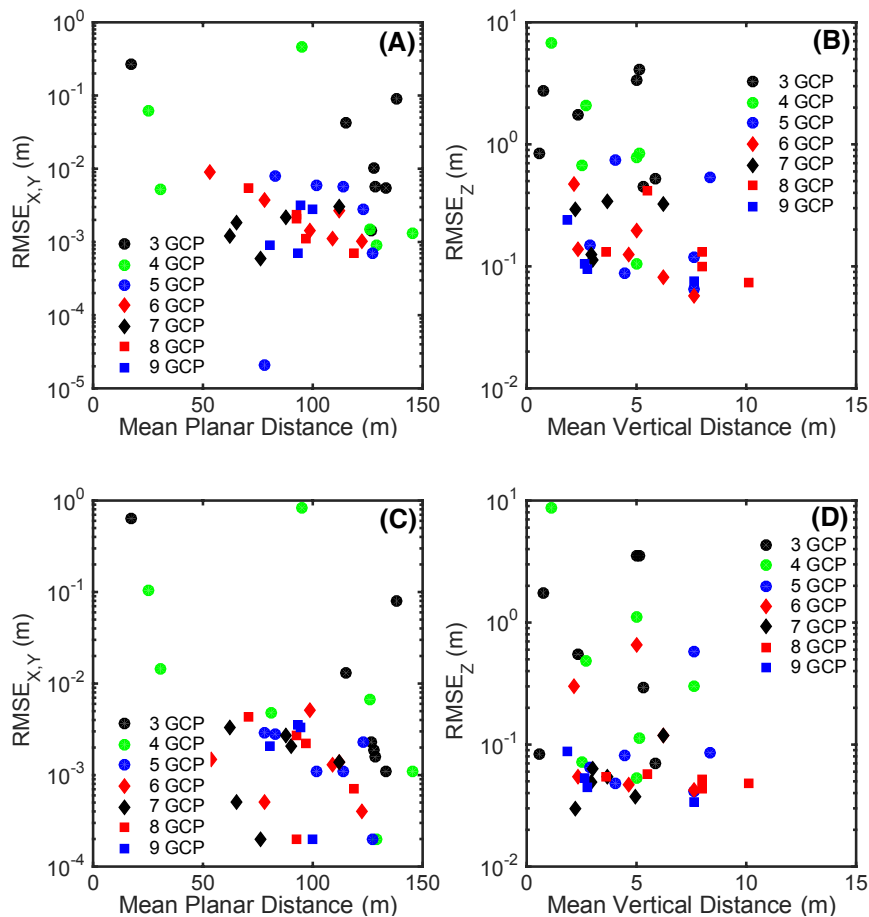
257

258   **Figure 7.** RMSE of the 3D model as a function of the mean distance between GCPs obtained for the
259   flight N.2 (A, B) and for the combination of flights N.1 and N.4 (C, D).

4. Discussions

261   UAS-derived 3D models provide a new strategy to monitor land surface with an extremely high
262   level of detail. The literature does not provide clear guidelines about operational use of UAS for 3D
263   model reconstruction based on SfM-MVS algorithms, but several researchers explored different
264   strategies aimed at minimizing the errors of 3D models. Review of these studies is extremely
265   instructive to identify the control excerpted by the GCPs density on the planar and vertical accuracy
266   of UAS-derived DSMs. Planar accuracy of SfM-MVS outputs are generally higher than vertical
267   precision. This result impacts on the mean number of GCPs needed to improve the overall quality of
268   the 3D model. In general, 5 GCPs/ha are enough to reach good performances on the plane, but 10
269   GCPs/ha are need to reach good precision in elevation (see Figure 1). Nevertheless, the final result is
270   highly influenced by a number of factors such as flight pattern and configuration, camera quality,
271   and local morphological complexity.
272   In our analysis, we focused on the 3D model optimization exploiting the combination of different
273   flight configurations and the optimal GCPs design. For this reason, we explored the impact of : 1) the

274 combined use of images obtained from different flight patterns and configurations, and 2) the use of
275 a variable number of GCPs. Both approaches are already used in practical application, still without
276 clear identification of the benefits associated with combining images acquired using different flight
277 plans and camera settings, nor the quantification of the impact of such choices. In addition, the
278 density and distribution of GCPs remain open and not fully addressed.
279   According to our results it seems clear that the mission planning represents critical preliminary
280 step that may significantly affect the final results. At certain circumstances, well-defined single flight
281 may be sufficient to reach a fairly good quality of the overall survey. Nevertheless, the combination
282 of flights with differing configurations can retrieve information from different viewpoints and angles
283 that can certainly increase resulting accuracy. Given the optical nature of SfM-MVS algorithms, the
284 challenge is to maximize the number of observations of each individual point retrieved across the
285 area of interest. In this, the use of tilted camera may be beneficial in order to improve robustness of
286 the geometrical model increasing the number of tie points describing inclined surfaces. Tilt of the
287 camera should be defined according to both local morphology and resolution required. For the
288 studied case characterized by trapezoidal earthen dam with an elevation of about 10 m and gentle
289 slopes with elevation changes of 15 m, a tilt of 20° combined with a 0° flight were the best performing.
290 This result can be justified by taking a closer look at the results reported on the diagonal of Table 3.
291 In fact, the accuracy of planar coordinates is generally higher when using a nadir camera settings
292 with lower flight altitude, but the vertical error is always lower for the flight with a 20° tilted camera.
293 Therefore, the combination of the two flights tends to optimize both characteristics of DSMs.
294   The flights operated on two orthogonal routes provided additional benefits to the description of
295 the area allowing a relevant reduction of error (for comparison see results of the combination 1 - 2).
296 Comparing the accuracy of different DSMs obtained with a single flight or a combination of flights,
297 the flight combination and tilted camera significantly increased the vertical accuracy, providing clear
298 benefits to the process of DSM construction.
299   The error magnitude is also influenced by the flight altitude that controls image resolution. The
300 use of multiple flights at different flight altitudes is a common practice to improve survey accuracy
301 in aerophotogrammetry. We also observed a beneficial effect on the relative elevation accuracy of
302 DSM, but such improvement is probably also influenced by the lower resolution of the images and
303 in general is less effective than the use of a 20°tilted camera. Also in the literature, there are
304 contrasting results on the relative impact of flight altitude, e.g. Gómez-Candón et al. [17] showed
305 weak relationship of RMSE and flight height.
306   Orthorectification of orthomosaics is traditionally performed using GCPs, still other options
307 should also be considered, such as investing in carrier phase GPS receiver and processing workflow
308 that can help to reduce the amount of fieldwork needed in terms of GCP collection [24], especially
309 useful if monitoring larger areas.
310   The new SfM-MVS algorithms have been markedly improving capabilities in construction of 3D
311 models, but still the minimum number of GCPs needed to reach specific quality is uncertain. For
312 example, Singth et al. [23] described weak negative relationship between GCPs and root mean square
313 error (RMSE). Generally, at least three GCPs are necessary to allow the SfM-MVS algorithms to take
314 advantage of such information. James et al. [10] recommend minimum of four to five GCPs, and
315 emphasize accurate camera calibration, a factor not considered in our research. They showed that
316 high RMSE for three GCPs decreases markedly for six GCPs especially for vertical component.
317   Our results show that with increasing number of GCPs there is an increase in quality of the 3D
318 model that can reach values of few centimeters of planar RMSE (about 0.2cm) already for five GCPs.
319 Vertical quality is generally lower, reaching centimeter precision (about 4cm) only if more than seven
320 GCPs and two flights are adopted. This discrepancy of optimum number of GCPs recommended by
321 different studies can partly be explained by the fact that for small number of GCPs, the error can be
322 strongly influenced by their spatial distribution [10]. Indeed our results show that the spatial
323 distribution of GCPs strongly controls the DSM accuracy, increasing with the mean GCP distance.
324 This suggests that GCPs should be spread in space as much as possible to cover the entire range of
325 variability in elevation and fulfil the extent of the area. These results corroborate the findings of James

326   and Robson [25] and Smith et al. [10] suggesting distribution of GCPs across and at the edges of the
327   target area.

5. Conclusion

329   In the present manuscript, we tried to delineate some guidelines for UAS- surveys aimed at the
330   derivation of 3D surface models. Exploiting the available literature on this topic and our field
331   experiences, a number of indication can be derived:

- First of all the morphological complexity of the studied site represents the major difficulty for the surveys. The relevant changes observed in different study cases are mainly influenced by this factor. Nevertheless, accuracy can be improved increasing the number of GCPs, but elevation precision is the most challenging parameter.
- Flight pattern may significantly impact the result of the analysis. Therefore, it should be planned thoroughly to achieve the best vision of the entire area. Transversal survey with respect to a given structure provides a better description and quality of the resulting 3D surface.
- The use of images derived from different flights may be beneficial for DSM accuracy. In particular, the use of a tilted camera can improve the amount of information (retrieved number of points) for inclined surfaces providing higher DSM elevation accuracy. The presence of tilted camera images produces an increased robustness of the geometrical model providing a possible strategy to reduce the total number of GCPs adopted over a given area.
- The RMSE of the resulting 3D model reaches the value of few centimeters both in the plane and in vertical with minimal number of seven GCPs. This result must be considered site specific.
- Finally, we observed that the quality of the 3D model tends to increase when both relative plane and vertical distance of GCPs increases, suggesting potential strategy for their distribution in space. As a consequence, it is convenient to spread them in space as much as possible these points.

353   The experiment described herein cannot be considered exhaustive; still it provides insights into
354   the problematic and can serve as a guideline for future applications. It is highly desirable to extend
355   the analysis to new case studies and landscape morphologies in order to provide clear and more
356   detailed guidelines for UAS applications. Nevertheless, the outcomes of the research lead to a number
357   of useful contents that can support and guide UAS applications event in different morphological
358   conditions. It is clear that there is not a unique response for the optimal number of GCPs that can
359   optimize a survey, but our analysis helped understanding some general concepts. For instance, we
360   should plan carefully our flights in order to optimize the amount of information retrieved by our
361   cameras and also that the use of combined flight patterns can significantly improve the overall quality
362   of the 3D models. That bears true even for the most critical dimension, which is the vertical one.

374

Appendix A: Dataset

In the present section, some of the most critical data derived from our analysis is reported in order to provide a full overview of the results and to give the possibility to readers to repeat some of the analysis reported herein. In the following, the tables with a list of the main characteristics of each SfM run are reported.

Number of GCP	RMSE$_{X,Y}$ (m)	RMSE$_Z$ (m)	RMSE$_Z$ (relative) (m)	Mean Planar distance (m)	Max Planar distance (m)	Mean Vertical distance (m)	Total distance (m)
2	184.070	55.100	40.920	8.45	8.45	2.17	10.61
2	57.540	18.580	30.630	40.34	40.34	0.09	40.43
2	24.7905	28.2890	10.2409	175.71	175.71	7.61	183.32
2	238.990	40.300	44.610	13.78	13.78	2.70	16.48
2	31.600	14.730	25.650	211.09	211.09	7.97	219.06
2	71.820	35.970	57.820	8.14	8.14	1.63	9.77
3	0.0892	2.1870	3.3477	138.22	207.32	5.03	143.25
3	0.265	5.910	4.070	17.39	26.05	5.11	22.50
3	0.010	0.726	1.735	127.78	191.33	2.36	130.14
3	0.0432	2.0284	2.7390	115.12	172.64	0.73	115.85
3	0.0058	0.3885	0.8351	128.19	191.44	0.57	128.76
3	0.0014	0.2904	0.5285	126.77	189.92	5.84	132.61
3	0.0055	0.4824	0.4484	133.18	177.09	5.30	138.48
4	0.0013	0.1028	0.1059	145.15	207.32	5.03	150.17
4	0.0053	0.9884	0.8459	30.78	49.51	5.11	35.89
4	0.0621	3.0553	2.0936	24.93	44.10	2.72	27.65
4	0.0009	0.2744	0.6726	129.22	226.61	2.55	131.77
4	0.03572	0.6726	0.6717	80.90	143.71	7.64	88.54
4	0.0015	0.4587	0.7903	125.73	207.32	5.03	130.76
4	0.4599	3.4737	6.8429	95.34	175.36	1.10	96.44
5	0.0058	0.7831	0.7491	113.61	209.12	4.05	117.66
5	0.00002	0.0315	0.0875	78.17	128.58	4.48	82.64
5	0.006	0.155	0.150	101.80	209.12	2.86	104.67
5	0.0028	0.1051	0.1182	123.03	226.61	7.61	130.64
5	0.0007	0.0439	0.0645	127.36	226.61	7.61	134.97
5	0.0079	0.5286	0.5332	83.05	143.71	8.32	91.38
6	0.0027	0.0442	0.0812	112.30	177.09	6.20	118.50
6	0.001	0.044	0.058	122.49	226.61	7.61	130.09
6	0.0014	0.0834	0.1949	98.83	207.32	5.03	103.85
6	0.0011	0.1074	0.1255	109.03	209.12	4.64	113.67
6	0.0038	0.1690	0.4740	77.91	177.09	2.18	80.09
6	0.0091	0.3059	0.1374	53.03	88.69	2.36	55.38
7	0.0020	0.0560	0.1200	90.08	209.12	4.94	95.02
7	0.003	0.044	0.327	112.30	177.09	6.20	118.50
7	0.0018	0.1455	0.2936	65.48	133.10	2.22	67.70
7	0.0022	0.1063	0.1257	87.51	211.09	2.92	90.43
7	0.0006	0.0934	0.1137	75.94	176.51	3.03	78.97
7	0.0012	0.3035	0.3379	62.35	93.08	3.65	66.00
8	0.0007	0.0506	0.0730	118.79	226.61	10.09	128.88
8	0.0021	0.1305	0.1316	92.43	226.61	3.62	96.05
8	0.0055	0.2573	0.4162	70.48	135.95	5.52	75.99
8	0.0024	0.0804	0.1318	92.79	211.09	7.97	100.76
8	0.0011	0.0905	0.0999	96.91	211.09	7.97	104.88
9	0.0028	0.0310	0.0747	99.71	226.61	7.61	107.32
9	0.0009	0.1258	0.2393	80.41	177.09	1.86	82.27
9	0.0031	0.0678	0.1045	94.67	211.09	2.64	97.30
9	0.0007	0.0812	0.0950	93.34	191.44	2.75	96.09

Table 4. Characteristics of the different SfM-MVS runs carried out with the dataset obtained from flight N.2.

Number of GCP	RMSE$_{X,Y}$ (m)	RMSE$_Z$ (m)	RMSE$_Z$ (relative) (m)	Mean Planar distance (m)	Max Planar distance (m)	Mean Vertical distance (m)	Total distance (m)
2	567.6526	76.9213	52.8201	8.45	8.45	2.17	10.61
2	54.4840	17.8242	30.8395	40.34	40.34	0.09	40.43
2	34.5736	30.2337	10.9425	175.71	175.71	7.61	183.32
2	275.0078	53.0793	57.9899	13.78	13.78	2.70	16.48
2	35.1901	15.1104	26.3944	211.09	211.09	7.97	219.06
2	70.2968	30.6586	42.1679	8.14	8.14	1.63	9.77
3	0.0806	2.3228	3.5662	138.22	207.32	5.03	143.25
3	0.6367	5.9248	3.5594	17.39	26.05	5.11	22.50
3	0.0019	0.2025	0.5453	127.78	191.33	2.36	130.14
3	0.0129	1.2650	1.7613	115.12	172.64	0.73	115.85
3	0.0016	0.0577	0.0826	128.19	191.44	0.57	128.76
3	0.0023	0.0286	0.0702	126.77	189.92	5.84	132.61
3	0.0011	0.2517	0.2947	133.18	177.09	5.30	138.48
4	0.0011	0.0206	0.0532	145.15	207.32	5.03	150.17
4	0.0146	0.1483	0.1143	30.78	49.51	5.11	35.89
4	0.1026	0.6844	0.4832	24.93	44.10	2.72	27.65
4	0.0002	0.0530	0.0726	129.22	226.61	2.55	131.77
4	0.0048	0.3018	0.3003	80.90	143.71	7.64	88.54
4	0.0068	0.8508	1.1049	125.73	207.32	5.03	130.76
4	0.8313	4.3809	8.6589	95.34	175.36	1.10	96.44
5	0.0011	0.0616	0.0644	101.80	209.12	2.86	104.67
5	0.0023	0.4664	0.5754	123.03	226.61	7.61	130.64
5	0.0002	0.0320	0.0413	127.36	226.61	7.61	134.97
5	0.0028	0.0845	0.0852	83.05	143.71	8.32	91.38
5	0.0011	0.0540	0.0485	113.61	209.12	4.05	117.66
5	0.0029	0.0311	0.0806	78.17	128.58	4.48	82.64
6	0.0014	0.0394	0.1176	112.30	177.09	6.20	118.50
6	0.0004	0.0295	0.0423	122.49	226.61	7.61	130.09
6	0.0052	0.6343	0.6602	98.83	207.32	5.03	103.85
6	0.0013	0.0345	0.0464	109.03	209.12	4.64	113.67
6	0.0005	0.0302	0.3019	77.91	177.09	2.18	80.09
6	0.0015	0.0315	0.0542	53.76	88.69	2.36	56.12
7	0.0021	0.0437	0.0370	90.08	209.12	4.94	95.02
7	0.0014	0.0394	0.1176	112.30	177.09	6.20	118.50
7	0.0005	0.0374	0.0300	65.48	133.10	2.22	67.70
7	0.0027	0.0304	0.0497	87.51	211.09	2.92	90.43
7	0.0002	0.0335	0.0627	75.94	176.51	3.03	78.97
7	0.0033	0.0558	0.0548	62.35	93.08	3.65	66.00
8	0.0007	0.0290	0.0483	118.79	226.61	10.09	128.88
8	0.0044	0.0235	0.0569	70.48	135.95	5.52	75.99
8	0.0027	0.0275	0.0513	92.79	211.09	7.97	100.76
8	0.0022	0.0312	0.0432	96.91	211.09	7.97	104.88
8	0.0002	0.0496	0.0542	92.43	226.61	3.62	96.05
9	0.0002	0.0144	0.0341	99.71	226.61	7.61	107.32
9	0.0021	0.0365	0.0883	80.41	177.09	1.86	82.27
9	0.0033	0.0302	0.0528	94.67	211.09	2.64	97.30
9	0.0035	0.0373	0.0444	93.34	191.44	2.75	96.09

Table 5. Characteristics of the different SfM-MVS runs carried out with the dataset obtained from flights N.1 – N.4.

The relative differences between the SfM-MVS runs with a single and two flights are summarized in Table 5. In particular, we report the mean value and the standard deviation of the RMSE obtained using the two datasets with differing numbers of GCPs. In this table, the advantage

391 in using a combination of flight configurations is obvious. It is mainly related to a significant
392 reduction of the vertical error of the UAS-derived DSM.
393

Number of GCPs/RMSE	Dataset from Flight N.2								
	1	2	3	4	5	6	7	8	9
Mean RMSE$_{X,Y}$ (m)	440.14	101.46	0.060	0.088	0.004	0.0032	0.0018	0.0024	0.0019
STD RMSE$_{X,Y}$ (m)	277.93	88.66	0.095	0.183	0.003	0.0031	0.0009	0.0019	0.0013
Mean RMSE$_Z$ (m)	30.25	32.16	1.716	1.392	0.274	0.1257	0.1385	0.1219	0.0764
STD RMSE$_Z$ (m)	10.89	14.90	2.008	1.486	0.309	0.0998	0.0991	0.0809	0.0392
Mean total RMSE (m)	33.44	34.97	1.957	1.892	0.283	0.1785	0.2396	0.1705	0.1284
STD total RMSE (m)	8.53	16.53	1.451	2.512	0.286	0.1524	0.1107	0.1395	0.075
	Dataset from Flights N.1 and N. 4								
Mean RMSE$_{X,Y}$ (m)	680.65	172.87	0.105	0.137	0.002	0.0017	0.0017	0.002	0.0023
STD RMSE$_{X,Y}$ (m)	175.85	213.96	0.236	0.308	0.001	0.0018	0.0012	0.0017	0.0015
Mean RMSE$_Z$ (m)	33.81	37.30	1.436	0.920	0.122	0.1332	0.0400	0.0322	0.0296
STD RMSE$_Z$ (m)	14.24	23.60	2.151	1.559	0.170	0.2455	0.0090	0.0101	0.0106
Mean total RMSE (m)	37.62	36.86	1.411	1.541	0.149	0.2037	0.0586	0.0508	0.0549
STD total RMSE (m)	11.41	17.59	1.578	3.160	0.210	0.2444	0.0312	0.0053	0.0235

394   **Table 6.** The mean and standard deviation of the estimated RMSE depending on the number of GCPs.

395 **References**

396 1. Colomina, I.; Molina, P. Unmanned aerial systems for photogrammetry and remote sensing: A review.
397   *ISPRS J. Photogramm. Remote Sens.* **2014**, 92, 79–97, doi: 10.1016/j.isprsjprs.2014.02.013.
398 2. Whitehead, K.; Hugenholtz, C.H.; Myshak, S.; Brown, O.; LeClair, A.; Tamminga, A.; Barchyn, T.E.;
399   Moorman, B.; Eaton, B. Remote sensing of the environment with small unmanned aircraft systems (UASs),
400   part 2: Scientific and commercial applications. *J. Unmanned Veh. Syst.* **2014**, 2, 86–102, doi:10.1139/juvs-2014-
401   0006.
402 3. Manfreda, S.; McCabe, M.F.; Miller, P.; Lucas, R.; Pajuelo Madrigal, V.; Mallinis, G.; Ben Dor, E.; Helman,
403   D.; Estes, L.; Ciraolo, G.; Müllerová, J.; Tauro, F.; De Lima, M.I.; De Lima, J.L.; Frances, F.; Caylor, K.; Kohv,
404   M.; Maltese, A.; Perks, M.; Ruiz-Pérez, G.; Su, Z.; Vico, G.; Toth, B. On the Use of Unmanned Aerial Systems
405   for Environmental Monitoring. *Remote Sens.* **2018**, 10(4), 641; doi:10.3390/rs10040641.
406 4. Lucieer, A.; Jong, S. M. D.; & Turner, D. Mapping landslide displacements using Structure from Motion
407   (SfM) and image correlation of multi-temporal UAV photography. Progress in Physical Geography **2014**,
408   38(1), 97-116.
409 5. Clapuyt, F.; Vanacker, V.; Van Oost, K. Reproducibility of UAV-based earth topography reconstructions
410   based on Structure-from-Motion algorithms. *Geomorphology* **2016**, 260, 4-15, doi:
411   10.1016/j.geomorph.2015.05.011.
412 6. Cook, S.J.; Clarke, L.E.; Nield, J.M., Geomorphological Techniques (Online Edition). British Society for
413   Geomorphology, London. ISSN: 2047-0371, **2012**.
414 7. Westoby, M. J.; Brasington, J.; Glasser, N. F.; Hambrey, M. J.; Reynolds, J. M. 'Structure-from-Motion'
415   photogrammetry: A low-cost, effective tool for geoscience applications. *Geomorphology* **2012**, 179, 300-314,
416   doi: 10.1016/j.geomorph.2012.08.021.
417 8. Carrivick, J. L.; Smith, M. W. Quincey, D. J. Structure from Motion in the Geosciences. John Wiley & Sons,
418   **2016**.
419 9. Smith, M.W.; Vericat, D. From experimental plots to experimental landscapes: topography, erosion and
420   deposition in sub-humid badlands from structure-from-motion photogrammetry. *Earth Surf. Process. Landf.*
421   **2015**, 40 (12), 1656–1671, doi: 10.1002/esp.3747.

10. James, M. R.; Robson, S.; d'Oleire-Oltmanns, S.; Niethammer, U. Optimising UAV topographic surveys processed with structure-from-motion: Ground control quality, quantity and bundle adjustment. *Geomorphology* **2017**, 280, 51-66, doi: 10.1016/j.geomorph.2016.11.021.

11. Ridolfi, E.; Buffi, G.; Venturi, S.; Manciola, P. Accuracy Analysis of a Dam Model from Drone Surveys. Sensors **2017**, 17, 1777, doi:10.3390/s17081777.

12. Rock, G.; Ries, J. B.; & Udelhoven, T. Sensitivity analysis of UAV-photogrammetry for creating digital elevation models (DEM). In Proceedings of Conference on Unmanned Aerial Vehicle in Geomatics **2011**.

13. Tahar, K. N. An evaluation on different number of ground control points in unmanned aerial vehicle photogrammetric block. *Int. Arch. Photogramm. Remote Sens. Spat. Inf. Sci* **2013**, 40, 93-98, doi: 10.3390/ecrs-2-05165.

14. Mancini, F.; Dubbini, M.; Gattelli, M.; Stecchi, F.; Fabbri, S.; Gabbianelli, G. Using unmanned aerial vehicles (UAV) for high-resolution reconstruction of topography: The structure from motion approach on coastal environments. *Remote Sensing* **2013**, 5(12), 6880-6898, doi:10.3390/rs5126880.

15. Hugenholtz, C.H.; Whitehead, K.; Brown O.W.; Barchyn, T.E.; Moorman, B.J.; LeClair, A.; Riddell, K., Hamilton, T. Geomorphological mapping with a small unmanned aircraft system (sUAS): Feature detection and accuracy assessment of a photogrammetrically-derived digital terrain model. *Geomorphology* **2013**, 194: 16-24. doi: 10.1016/j.geomorph.2013.03.023.

16. Cryderman, C.; Mah, S. B.; Shufletoski, A. Evaluation of UAV photogrammetric accuracy for mapping and earthworks computations. *Geomatica* **2014**, 68(4), 309-317, doi: 10.5623/cig2014-405.

17. Gómez-Candón, D.; De Castro, A. I.; López-Granados, F. Assessing the accuracy of mosaics from unmanned aerial vehicle (UAV) imagery for precision agriculture purposes in wheat. *Precision Agriculture* **2014**, 15(1), 44-56.

18. Uysal, M.; Toprak, A. S.; & Polat, N. DEM generation with UAV Photogrammetry and accuracy analysis in Sahitler hill. Measurement **2015**, 73, 539-543.

19. Küng, O.; Strecha, C.; Beyeler, A.; Zufferey, J. C.; Floreano, D.; Fua, P.; & Gervaix, F. The accuracy of automatic photogrammetric techniques on ultra-light UAV imagery. In UAV-g 2011-Unmanned Aerial Vehicle in Geomatics **2011** (No. EPFL-CONF-168806).

20. Agüera-Vega, F.; Carvajal-Ramírez, F.; & Martínez-Carricondo, P. Assessment of photogrammetric mapping accuracy based on variation ground control points number using unmanned aerial vehicle. *Measurement* **2017**, 98, 221-227, doi: 10.1016/j.measurement.2016.12.002.

21. Koci, J.; Jarihani, B.; Leon, J. X.; Sidle, R. C.; Wilkinson, S. N.; & Bartley, R. Assessment of UAV and ground-based Structure from Motion with multi-view stereo photogrammetry in a gullied savanna catchment. ISPRS International Journal of Geo-Information **2017**, 6(11), 328.

22. Oniga, V.-E.; Breaban, A.-I.; Statescu, F. Determining the Optimum Number of Ground Control Points for Obtaining High Precision Results Based on UAS Images. *Proceedings* **2018**, 2, 352, doi: 10.3390/ecrs-2-05165.

23. Singh, K. K.; Frazier A.E. A meta-analysis and review of unmanned aircraft system (UAS) imagery for terrestrial applications, *Int. J. Remote Sens.* **2018**, doi: 10.1080/01431161.2017.1420941

24. Müllerová, J.; Bartaloš, T.; Brůna, J.; Dvořák, P.; & Vítková, M. Unmanned aircraft in nature conservation – an example from plant invasions. *Int. J. Remote Sens.* **2017**, 38 (8-10): 2177-2198; doi: 10.1080/01431161.2016.1275059

25. James, M.R.; Robson, S. Straightforward reconstruction of 3D surfaces and topography with a camera: Accuracy and geoscience application. *J. Geophys. Res. Earth Surf.* **2012**, 117, F03017.